Any correspondence concerning this service should be sent
to the repository administrator: tech-oatao@listes-diff.inp-toulouse.fr

$Ln_2NiO_{4+\delta}$ (Ln = La, Pr, Nd) coatings deposited by reactive magnetron sputtering as cathode material for intermediate temperature solid oxide fuel cell

J. Fondard [a, b], A. Billard [a, b], G. Bertrand [c], P. Briois [a, b, *]

[a] FEMTO-ST Institute (UMR CNRS 6174), Univ. Bourgogne Franche-Comté, UTBM, 2 Place Lucien Tharradin, F-25200 Montbéliard Cedex, France
[b] FR FCLab 3539, 90000 Belfort, France
[c] CIRIMAT UMR5085, ENSIACET, 4 allée E. Monso, 31030 Toulouse, France

ABSTRACT

This work focuses on the comparison of Ln Ni O coatings (Ln = La, Nd, Pr) deposited by reactive magnetron sputtering using Plasma Emission Monitoring (PEM) which allows high deposition rate. Each layer is deposited by different steps. The optimal regulation setpoint for oxide rare earth deposition is determined and then the current dissipated on the nickel target is adjusted to obtain the convenient Ln/Ni ratio and to achieve the K_2NiF_4 structure. After an appropriate annealing treatment, all coatings exhibit crystalline structures, which depend on the Ln/Ni ratio. Due to the instability of Pr_2NiO_4 structure at intermediate temperatures, the crystallization step of praseodymium nickelate is performed at higher temperature than the other materials. This further thermal treatment implies a more porous structure. Each coating exhibits interesting properties. Electrical and electrochemical characterizations performed on these deposits prove better properties of the praseodymium nickelate coating.

1. Introduction

The last generation of Solid Oxide Fuel Cells at intermediate temperature (IT SOFC), is dedicated to work around 873−1073 K in order to increase the lifetime of the various materials and to decrease the cost in use. Nevertheless, the low working tempera ture causes a drop of the cell performances, especially at the cathode side where the overpotential increases. A Mixed Ionic and Electronic Conductive oxide (MIEC) is regarded as potential mate rial solution to be implemented at these intermediate tempera tures. This kind of oxides present very good catalytic properties towards the oxygen and they are chemically compatible with the electrolyte and the interconnector. Most of the studies concerning MIECs are referred to perovskite type oxides [1–4] and place it as the reference for cathode materials for intermediate temperatures. The K_2NiF_4 structure materials are also interesting for this

application. Different Ln_2NiO_4 compounds (Ln La, Nd or Pr) with a large oxygen over stoichiometry in the whole temperature range 0−1173 K were studied. Their ionic conductivity, as well as their capacity to adsorb and to diffuse easily the oxygen within its structure (coefficients k, D*) are better than those of the usual cathode materials (Table 1). Their thermal expansion coefficient (TEC) is close to that of the usually used electrolyte materials (13 $10^{-6} K^{-1}$, 12.7 $10^{-6} K^{-1}$, 13.6 $10^{-6} K^{-1}$, 11.9 $10^{-6} K^{-1}$ and 11.6 $10^{-6} K^{-1}$ for $La_2NiO_{4+\delta}$, $Nd_2NiO_{4+\delta}$, $Pr_2NiO_{4+\delta}$, CeO_2 Gd_2O_3 (CGO) and ZrO_2 Y_2O_3 (YSZ) respectively). Moreover, their TEC value is very close to the one recorded for ferritic steel interconnect materials (11.0−12.5 $10^{-6} K^{-1}$) [9] which are connected in the last generation metal supported SOFC stack. $La_2NiO_{4+\delta}$ compounds are the most common nickelates and exhibit interesting electrochemical prop erties on half cells CGO and YSZ [5,10,11] and promising results in La_2NiO_4/LSGM/SDC/Ni−SDC complete cell [5]. Nd_2NiO_4 and $Nd_{1.95}NiO_4$ materials are also investigated in half cells [5,12,13]. These compounds were also tested in Ni CGO/TZ3Y/Nd_2NiO_4 [14] and Ni YSZ/YSZ/$Nd_{1.95}NiO_4$ [15] complete cells, demonstrating the feasibility of IT SOFCs by using these materials. Amongst all, numerous studies identified the Pr_2NiO_4 oxide as being one of the most promising materials for this application [5,16] or for oxygen

* Corresponding author. FEMTO-ST Institute (UMR CNRS 6174), Univ. Bourgogne Franche-Comté, UTBM, 2 Place Lucien Tharradin, F-25200 Montbéliard Cedex, France

E-mail address: pascal.briois@utbm.fr (P. Briois).

Table 1
Surface exchange (k) and oxygen diffusion coefficients (D*) for different cathode materials.

	D* (700 °C)	k (700 °C)
La_2NiO_4	$3.4\ 10^{-8}$ [5], $1.6\ 10^{-8}$ [6]	$1.7\ 10^{-7}$ [5], $1.3\ 10^{-7}$ [6]
Nd_2NiO_4	$5.0\ 10^{-8}$ [5]	$4.0\ 10^{-7}$ [5]
Pr_2NiO_4	$7.9\ 10^{-8}$ [5]	$1.7\ 10^{-6}$ [5]
LSCF	$3.2\ 10^{-9}$ [7], $7.2\ 10^{-9}$ [8]	$1.0\ 10^{-7}$ [7], $6.1\ 10^{-7}$ [8]

permeation membranes [17]. Excellent results were found from impedance measurements on $Pr_2NiO_{4+\delta}$/CGO/YSZ half cells [18] and enhanced the promising behavior of this compound. B. Phil ippeau et al. [19] compare each material in half cell configuration with YSZ, CGO and LSGM electrolytes. This study proves better characteristics of Pr_2NiO_4 material at 873 and 973 K.

Whereas thick layers deposited by wet deposition techniques are commonly used as cathodes in IT SOFCs, recent studies deal with the deposition of Mixed Ionic and Electronic Conductors (MIECs) thin layers by physical surface deposition processes [20−23]. Some other studies proved that a thin and dense cathode layer placed between the electrolyte and a porous cathode leads to the electrochemical performances enhancement due to the better cathode/electrolyte contact [24]. However, the use of a thin dense layer as SOFC cathode was not fully studied, but some researchers have began to work on this point [20]. In this context, the use of magnetron sputtering technique, which allows the deposition of: electrolyte [25,26], diffusion barrier layers [27,28] and even Ni YSZ anode [30] in fuel cells, seems to be a promising route for producing thin microstructures [29]. Previous studies, performed in our lab oratory, permitted to deposit a La_2NiO_4 cathode layer by co sputtering of several metallic targets using the Plasma Emission Monitoring system (PEM) [24,31−33].

In the present work, we compare Ln_2NiO_4 coatings (Ln La, Nd, Pr) deposited by reactive magnetron sputtering under unstable conditions using PEM [33,35]. This technique allows the deposition of coatings with high sputtering rate. In this work, the electrical conductivity of the nickelates films is measured by four points probe technique on annealed samples from 293 to 1273 K under static air. Electrochemical characteristics of the coatings are investigated by impedance spectroscopy from 923 to 1123 K. The goal of this work is to deposit thin and dense cathode layer by using reactive magnetron sputtering technique, in order to reduce the cathode overpotential in an IT SOFC and to identify which is the most suitable material for this application.

2. Experimental details

2.1. Deposition device

The experimental deposition device is a 100 L Alcatel SCM 650 sputtering chamber pumped down via a system combining XDS35i Dry Pump and a 5401CP turbo molecular pump. The sputtering chamber is equipped with three 200 mm in diameter magnetron targets and with a 620 mm in diameter rotating substrates holder parallel to the targets at a distance of about 110 mm. The La, Nd, Pr and Ni targets were supplied with a pulsed DC Advanced Energy dual generator allowing the control of the discharge current. The discharge current was fixed at 2.5 A on the Ln target and was varied on the Ni target to obtain the convenient composition of the K_2NiF_4 structure. The substrates were made of alumina and YSZ pellets as well as glass slides positioned on the substrates holder at 170 mm from its center point. Argon and oxygen flow rates were controlled with Brooks flowmeters and the pressure was measured using a MKS Baratron gauge. The deposition stage was monitored using a closed loop control PEM (Plasma Emission Monitoring) system relying on an optical emission spectroscopy device (OES) [37]. This technique is based on the measurement of the optical intensity of: 394.91, 418.00 and 430.36 nm for La, Pr, Nd emission lines emitted from a volume near the target. The signal is collected through an optical fiber and directed to a Ropper Scientific SpectraPro 500i spectrometer, with a 1200 groove mm^{-2} grating and a photo multiplier tube (Hamamatsu R 636). Then, the information is transferred to a computer where an in house software developed in Labview® monitors the oxygen flow rate to maintain the intensity of the optical signal I_{La}^* at a fixed value.

2.2. Structural, morphological and optical characterizations

The coatings morphology is characterized by Scanning Electron Microscopy (SEM) using a JEOL JSM 5800 LV equipped with Energy Dispersive Spectroscopy (EDS) for chemical measurements. The structural features of the coatings are identified in Bragg Brentano configuration X ray diffraction using a BRUKER D8 focus diffrac tometer ($CoK_{\alpha1+\alpha2}$ radiations) equipped with the LynxEye linear detector. X Ray Diffraction (XRD) patterns are collected at room temperature during 10 min in the [20°−80°] scattering angle range by a step of 0.019°. The coating thickness is determined using the "step" method (a small surface of the substrate is covered with a tape that is removed after deposition leaving a step due to the coating thickness) with an Altysurf profilometer from Altimet allowing an accuracy of about 20 nm. Before each mea surement, the calibration of the experimental device was realized with a reference sample number 787569 accredited by CETIM, France.

The optical transmittance measurements are performed with a UV−visible−NIR Shimadzu UV 3600 Spectrophotometer controlled by UV probe 2.33 software. All measurements are carried out on glass substrates between 380 and 780 nm.

2.3. Electrical measurements

The electrical resistivity measurements are performed with a HP 3458A multimeter on Ln Ni O films deposited on alumina sub strates. With regard to its high insulating character, it is assumed that the substrate has no significant contribution to the electrical conductivity. The four points probe technique with four Pt aligned electrodes is used. Two outer probes behave as the current carrying electrodes (I1, I2) and the two inner ones were used to measure the voltages (E1, E2). Two cell configurations were used for the mea surements. First cell, which is a standard and certified cell allowing the accurate determination of the geometric factor, was used to define the resistivity at room temperature (Jandel, Linslade, UK). The second cell, developed by the LEPMI laboratory (Grenoble, France), allows measurements at various temperatures. The cell is placed inside an alumina tube and positioned into a furnace (Pekly, Thions Gardais, France), in order to measure the electrical re sistivity for different temperatures. The comparison of the resis tance measured at room temperature with cell 1 and at intermediate temperatures (873−1073 K) with cell 2 can be used to determine the geometric factor of cell 2.

2.4. Electrochemical measurements

The impedance spectroscopy measurements of Ln_2NiO_4/YSZ symmetrical cells are performed with a Solartron 1260 impedance/gain phase analyzer. Samples are inserted inside a cell developed by the LEPMI laboratory (Grenoble, France) where one face is positioned on a platinum plate and a platinum grid is maintained on the other face to ensure electrical contact. The grid is linked on a

platinum wire connected to the measurement device. The grid surface allows to calculate the Area Specific Resistance (ASR) of the cathode layer. The cell is placed inside an alumina tube and positioned into a furnace (Pekly, Thions Gardais, France).

3. Deposition and characterization

3.1. Determination of the optimal regulation setpoint

By fixing the discharge current of a metallic target, its physico chemical state is usually monotonic and a quite proportional function of the optical signal I_M^* measured by OES [33]. When oxygen gas is added into the device, a characteristic hysteresis loop of the instability of the sputtering conditions appears (Fig. 1). So, the transition between fast metallic and slow ceramic deposition happens suddenly. The Plasma Emission Monitoring (PEM) system allows the deposition of coatings in unstable sputtering conditions by fixing the intensity of the plasma emission line of the target in a closed loop as explained in Ref. [34]. Indeed, PEM is a very suitable technique that allows high rate growth of oxide coatings [24,32,33,37] in comparison to deposition of the same oxide under stable conditions [25,31]. As the main element of Ln_2NiO_4 is Ln, the PEM control was performed on the La, Nd and Pr targets with a fixed 2.5 A discharge current in order to deposit coating with high sputtering rate without consuming too much the target. The argon flow rate is fixed at 50 sccm based on a previous study [32,33]. Fig. 1 shows the instability of the sputtering conditions. This figure presents the 395, 436 and 418 nm emission line intensity vs. oxygen flow rate for lanthanum (Fig. 1 a.), neodymium (Fig. 1b) and praseodymium (Fig. 1c) targets. Increasing or decreasing the oxygen flow rate produces a hysteresis loop. By using a low quantity of oxygen, metallic coating is deposited with high optical intensity and high discharge voltage. By increasing the oxygen flow rate up to

6.4, 7.1 and 5.8 sccm for La, Nd and Pr respectively, a drop in intensity happens implying the deposition of an oxide coating, because the entire target is oxidized. Above this point, oxide coating is deposited with a low deposition rate. The transition between the oxide and metallic mode happens at 2, 1.9 and 1.7 sccm respectively. Using PEM allows the deposition with a setpoint located in the unstable domain inside the hysteresis loop and allows the deposition of oxide coatings with higher deposition rates than with a fully poisoned target. The deposition of La_2NiO_4 coatings is described in previous studies [32–34] and will not be developed in details in this paper.

In first set of experiments, Ln O films are deposited on glass slides with different PEM setpoints (S) in order to deposit transparent films, revealing qualitatively their oxygen content [29]. The highest setpoint with no attenuation of the optical signal is desired because it is associated with higher deposition rate [32–37]. Fig. 2 shows the evolution of the optical transmission of La O (Fig. 2a), Nd O (Fig. 2b) and Pr O (Fig. 2c) coatings deposited with 2.5 A applied on targets with 50 sccm Ar flow rate. Some studies indicate that increasing the setpoint decreases the coating transparency and the stoichiometry of the TiO_2 and YSZ coatings [35,37]. This behavior is similar to that of La O (Fig. 2a) as explained in a previous study [34] and Nd O coatings (Fig. 2b). With neodymium oxide film, a regulation setpoint fixed at 50% produces no attenuation of the optical signal similar to that recorded for glass slide, which reveals the transparency of the coating (Fig. 2b). It becomes more and more attenuated with higher setpoints. Such a behavior means that the Nd O based film is metalloid saturated for setpoints lower than 50% and under stoichiometric for higher regulation points. In addition, the shape of the signal is slightly different around 540 and 580 nm because of the photo luminescent properties of this material, commonly used in LED. Nevertheless, the optical transmission evolves in a different way with the regulation
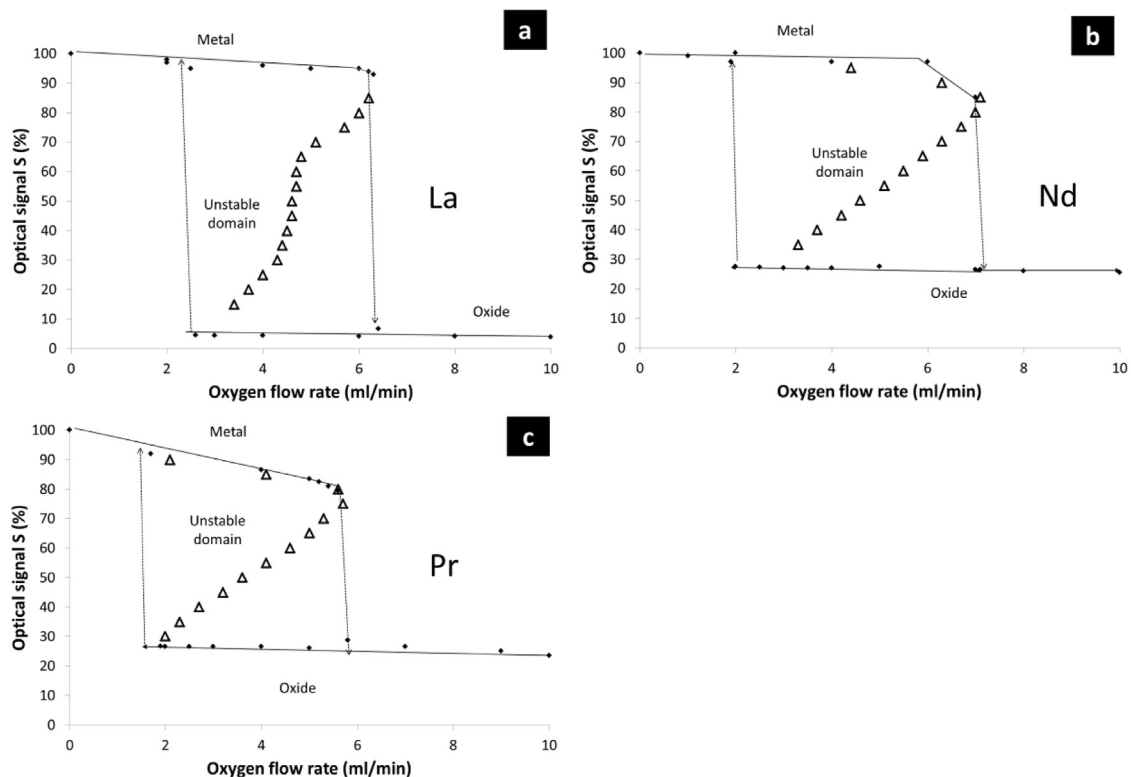

Fig. 1. Hysteresis loop of the different targets used with PEM system: La (a), Nd (b), Pr (c).
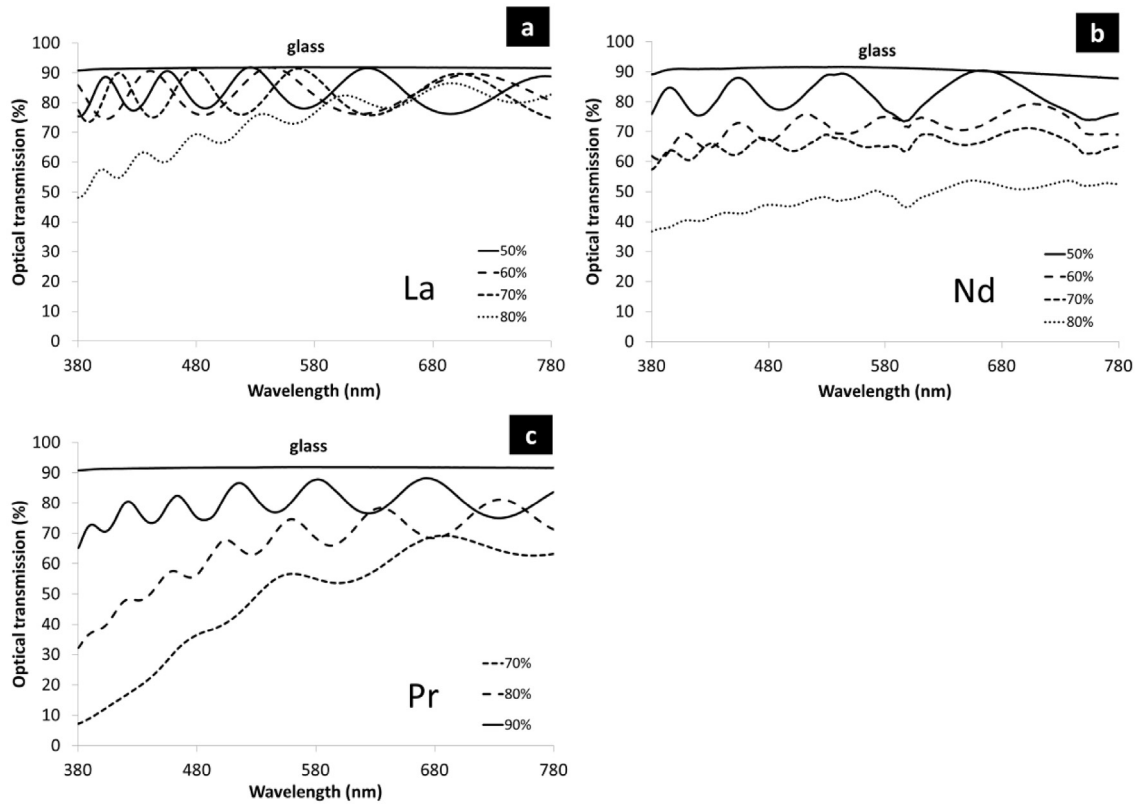
Fig. 2. Optical transmission vs. wavelength of Ln-O coatings. Ln   La (a), Nd (b), Pr (c).

setpoint for the Pr O film, where transparency decreases with the setpoint (Fig. 2c). Only the coating made with 90% regulation rate presents an unattenuated optical signal characteristic of a trans parent coating fully oxidized. Structural analysis performed on coatings deposited on glass slides allowed to identify the phases in presence and is presented in Fig. 3. This figure shows the formation of different structures with the different regulation setpoints (S). With S   70%, two phases are identified, a large peak of praseo dymium oxide (PrO_x) is present but it cannot be identified with our data. Moreover, metallic praseodymium is also identified. The amount of PrO_x decreases from a setpoint of 80% and cubic Pr_6O_{11} which is the most stable phase under air atmosphere and

hexagonal Pr_2O_3 appear. With S   90%, the amount of Pr_6O_{11} and metallic praseodymium phases increase. The different oxygen partial pressures cause the formation of the different praseodym ium oxides but the amount of oxygen is not sufficient to oxidize all the coatings for some deposition conditions and metallic praseo dymium appears. The hysteresis curve confirms this hypothesis because a 90% regulation point deposits metallic praseodymium which is unwanted to avoid strains during annealing (Fig. 1c). The most favorable condition seems to be a setpoint fixed at 80%.

The choice of the optimal deposition conditions is also dictated by the deposition rates of the coatings. Fig. 4 shows the evolution of the deposition rates with the setpoints. Deposition rates are in the
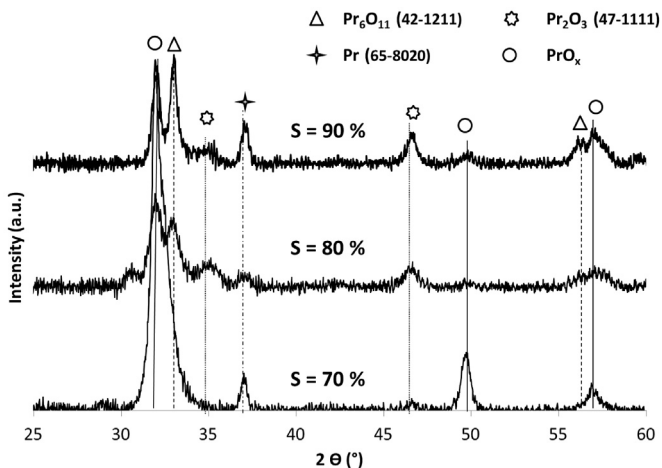

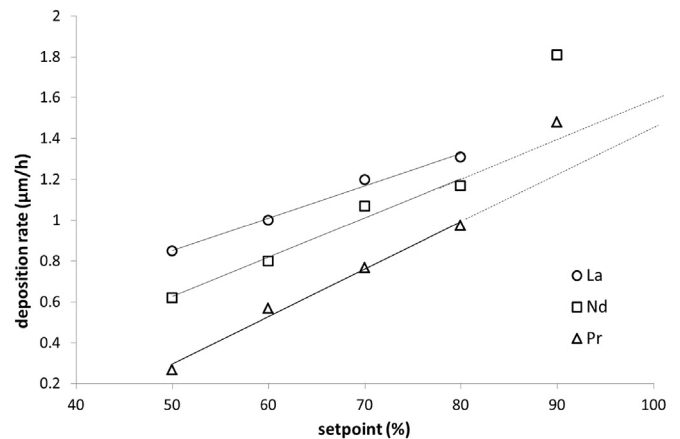**Fig. 3.** XRD measurements of Pr-O coatings as a function of the regulation setpoint.

Fig. 4. Deposition rate of Ln-O coatings as a function of the regulation setpoint. Ln   La (○), Nd (□), Pr (▲).

same order of magnitude and increase with the setpoint. Differ ences are due to the physical state of the target. In fact, when the set point decreases the oxygen partial pressure increases. With S 90%, the deposition rate is higher than the medium line. This is due to the deposition of metallic coatings in Elemental Sputtering Mode (stable domain) as shown in Fig. 1b and c. Finally, it was thus decided to realize the Pr O coatings with 80% regulation setpoint while it is not completely transparent but slightly under stoichiometric. A setpoint of 50% was then chosen with Nd target because it presents a good compromise between deposition rate and the stoichiometry of the coating.

3.2. Deposition of ln Ni O coatings

The experimental parameters for the films synthesis are sum marized in Table 2. The coatings are deposited by the co sputtering of Ln (Ln La, Nd, Pr) and Ni metallic targets under Ar O$_2$ atmo sphere where oxygen flow rate is controlled by the PEM system. Previous studies made with La$_2$NiO$_4$ coatings prove that the K$_2$NiF$_4$ structure is achieved for a La/Ni ratio close to 2 [24,29,30] after an appropriate annealing treatment. A similar behavior is observed for the different tested lanthanides. Fig. 5 presents the metallic Ln/Ni ratio determined by EDS analyses versus the applied discharge current on the Ni target, while the Ln target current is fixed at 2.5 A. The metallic ratio decreases linearly with the increase of the cur rent applied on the Ni target. The desired composition to obtain an Ln/Ni atomic ratio of 2 is approached for 0.57, 0.50 and 0.51 A for La, Nd and Pr respectively. During the co sputtering process, the dif ference between the atomic radii of Ln (186−247 p.m.) and Ni (149 p.m.) atoms would lead to an amorphous coating due to the confusion principle. This phenomenon imposes the realization of a crystallization annealing treatment which may saturate the film in oxygen. XRD performed on as deposited samples confirm the presence of an amorphous structure whatever the composition is (Fig. 6). In order to crystallize the convenient Ln$_2$NiO$_4$ phase, different annealing treatments are conducted with the samples whose metallic ratio Ln/Ni is close to 2. The annealing treatments are realized under air during 2 h, from 673 K to 1473 K, with a temperature step of about 50 K. Subsequently, the structural evo lution of these samples as a function of the temperature is deter mined by XRD measurements (Fig. 6). Fig. 6 shows the structure evolution of the Nd Ni O (Fig. 6a) and Pr Ni O samples (Fig. 6b). For each sample, the first crystalline phase appears at 873 and 673 K for Nd Ni O and Pr Ni O samples respectively. For Pr Ni O, the rather large full width at half maximum indicates that the crystallites present a nanometric size at this temperature. A previous study made with La Ni O coatings determined 1173 K as the ideal tem perature to obtain the K$_2$NiF$_4$ phase [24,32,33]. As shown in Fig. 6 a, the Nd Ni O coating, presenting a Nd/Ni ratio of about 2.2, follows this law. From 873 K, in our database, face centered orthorhombic Nd$_2$NiO$_4$ and Nd$_4$Ni$_3$O$_{9.85}$ phases present diffraction angles close to

Table 2
Main deposition conditions of the study.

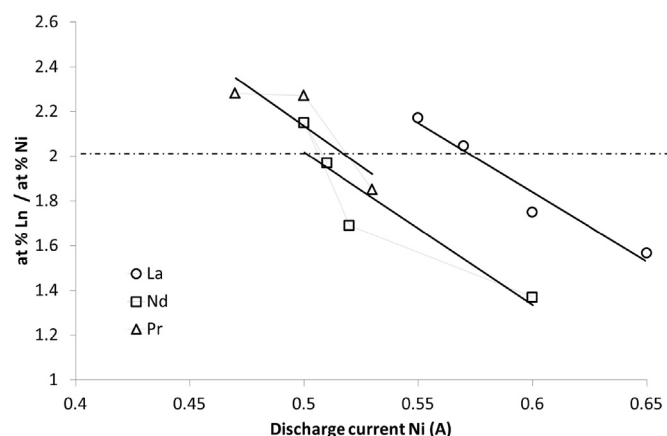| Parameters	La	Nd	Pr
Total pressure (Pa)	0.44	0.43 0.46	0.46
Argon flow rate (sccm)	50	50	50
Setpoint (%)	70	50	80
Oxygen flow rate (sccm)	4.5 4.9	4.5 5.2	4.5 4.8
Run duration (h)	2 2.2	2.5	2
Discharge current for La (A)	2.5	2.5	2.5
Frequency (Hz) toff (μs)	50 5	50 5	50 5
Discharge current for Ni (A)	0.55 0.65	0.4 0.6	0.47 0.53
Frequency (Hz) toff (μs)	50 5	50 5	50 5

Fig. 5. Evolution of atomic composition ratio Ln/Ni measured by EDS as a function of current dissipated on the Ni target (I$_{Ln}$ 2.5 A). Ln La (○), Nd (□), Pr (▲).

an unidentified Nd Ni O peak. From 1123 K, the wanted Nd$_2$NiO$_4$ phase crystallizes but still with Nd$_2$O$_3$ phase due to a slight excess of Nd material. The desired structure remains stable up to 1323 K, where the perovskite Nd$_4$Ni$_3$O$_{9.85}$ phase appears causing the disappearance of non conductive Nd$_2$O$_3$ phase. Nevertheless, Nd$_2$NiO$_4$ phase remains majority. So, 1173 K for 2h it has been found to be the optimal thermal treatment for Nd Ni O coating. XRD analysis with the convenient Nd/Ni ratio reveals that there was no presence of insulated phases after annealing at 1173 K (Fig. 5). The crystallization step is different with Pr Ni O films, presenting a Pr/ Ni ratio of about 2.3. On the temperature range from 673 to 1223 K, we observed the growth of Pr$_6$O$_{11}$ and Pr$_4$Ni$_3$O$_{9.85}$ without Pr$_2$NiO$_4$, usually appearing at 1173 K with other K$_2$NiF$_4$ structures. This is certainly due to the Pr$_2$NiO$_4$ decomposition. A similar phenomenon was observed in the literature below 1173 K [38,39]. In our study, the diffraction line of Pr$_2$NiO$_4$ phase appears between 1173 K and 1223 K. By increasing the temperature up to 1323 K, it is possible to reduce the Pr$_6$O$_{11}$ ratio in the coating. As a matter of fact, the heating up to 1423 K implied an onset of destabilization of the K$_2$NiF$_4$ structure. For this reason, the Pr$_2$NiO$_4$ phase is crystallized at 1323 K, even if the sample contains some impurities.

Morphological features of the coatings were performed by SEM observation of the surface and the brittle fracture cross sections on Nd$_2$NiO$_4$ (Fig. 7) and Pr$_2$NiO$_4$ coatings (Fig. 8), as deposited and fully oxidized by different annealing processes during 2 h. For both coatings, the observation of the surface of the as deposited films (Fig. 7 a and Fig. 8a) reveals the substrate morphology (alumina pellet) with an adherent and covering film. The adhesion of these films is pointed by the observation of the fracture of the films (Fig. 7 c and Fig. 8c) with a slightly columnar aspect. The thickness of these films is in agreement with profilometry measurements (i.e ≈ 2.0 and 2.2 μm for Nd and Pr nickelate films respectively). As expected after the analysis of La Ni O coating [32,33], the crystallization step allows the densification of the Nd Ni O coating (Fig. 7 b.and d) without cracks. A similar behavior is observed with Pr Ni O films after an 1173 K annealing (Fig. 8 b.and d). Nevertheless, films annealed at 1323 K present a completely different morphology and seem porous with the presence of grains with noodle shape (Fig. 8e). The observation of the cross section of these coatings confirms that they are not only porous on the surface but also in the thickness (Fig. 8f). A modification of the coating composition could explain the evolution of the morphology with the annealing treatment. Table 3 summarize the chemical composition of the film as deposited and after annealing treatment at 1173 K and 1323 K
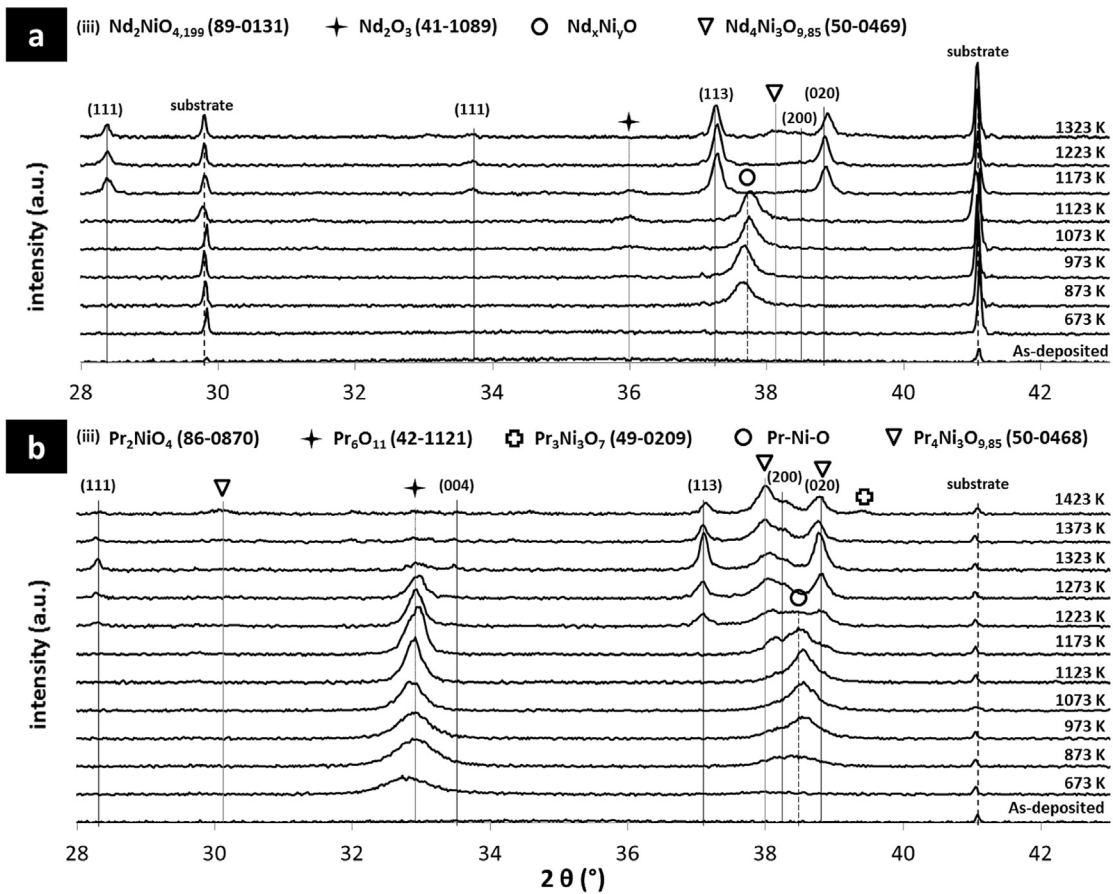
Fig. 6. Evolution of phase crystallization of Nd-Ni-O (a) and Pr-Ni-O (b) coatings as a function of annealing temperature during 2 h under air conditions.

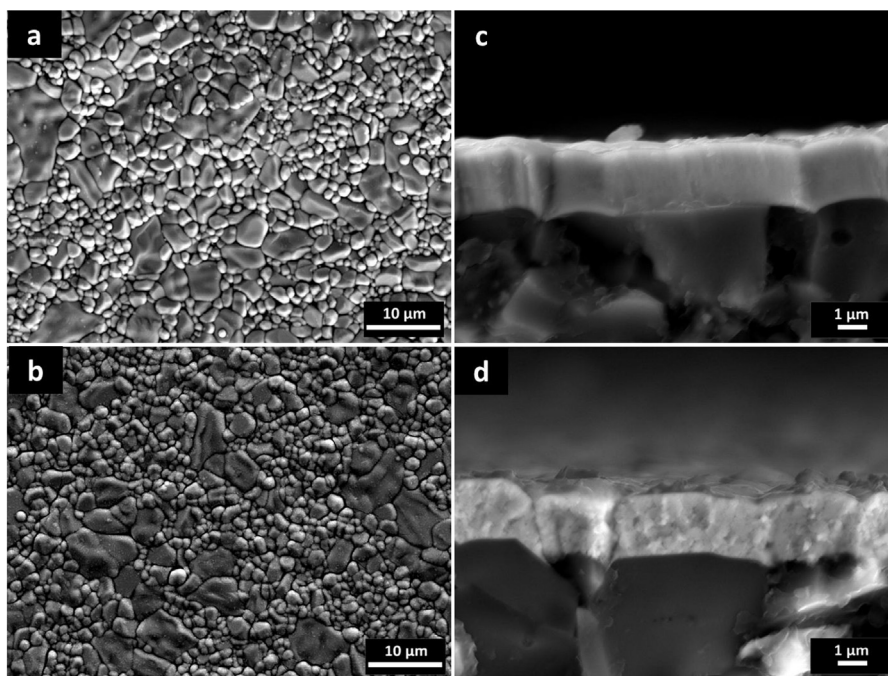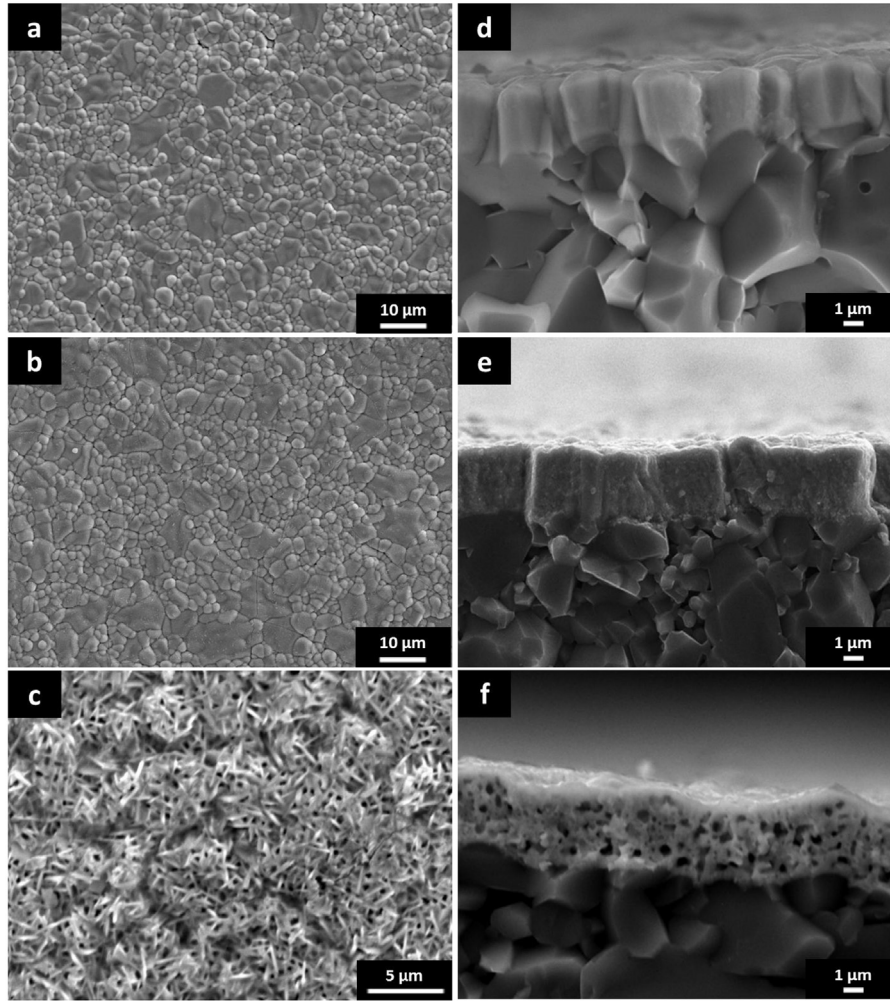**Fig. 7.** SEM view of surface of Nd_2NiO_4 samples as-deposited (a) and after crystallization (b) and brittle fracture cross section of as-deposited (c) and well-crystallized samples (d). The crystallization step is performed at 1173 K for 2 h.

Fig. 8. SEM view of surface of Pr_2NiO_4 samples as-deposited (a), after crystallization at 1173 k for 2 h (b), and after crystallization at 1323 k for 2 h (c). Brittle fracture cross section of samples as-deposited (d), after crystallization at 1173 k for 2 h (e), and after crystallization at 1323 k for 2 h (f).

Table 3
EDS measurements of K_2NiF_4 coatings as-deposited and annealed on YSZ support.

coating	Pr (at %) Ref: PrF3- Kα1 LaB6-Lα1	Ni (at %) Ref: Ni- Kα1	Pr/Ni
Pr_2NiO_4 (as-deposited)	69.63 ± 0.22	30.37 ± 0.22	2.29 ± 0.02
Pr_2NiO_4 (1223 K 2h)	69.45 ± 0.31	30.55 ± 0.31	2.27 ± 0.03
Pr_2NiO_4 (1323 K 2h)	67.51 ± 0.71	32.49 ± 0.71	2.07 ± 0.07

during 2 h. These compositions were performed by EDS measurements. The composition remains quite constant with the annealing treatment after an annealing at 1323 K. The difference in the Pr concentration is certainly induced by the modification of the layer morphology (Fig. 8f) and by the technique used to determine the concentration that is not sufficiently precise. The explanation that the morphology modification would be due to an evolution of the composition is confirm by the observation of brittle cross section after annealing at 1173 K (Fig. 8d). In spite of the destabilization of the K_2NiF_4 phase at this temperature, it is not possible to obtain dense Pr_2NiO_4 structure films by this method but the porous morphology (Fig. 8c and f) can be useful for the application of this layer as cathode layer in a solid oxide fuel cell.

These Ln_2NiO_4 (La, Nd, Pr) structures remain stable after an annealing at 973 K during 12 h on YSZ substrates, as shown in Fig. 9, validating the crystallization process. Fig. 9 highlights the samples purity. Lanthanum and neodymium nickelate coatings are almost pure (Fig. 9a, and c) while praseodymium nickelate sample contains small amount of $Pr_4Ni_3O_{9.85}$ perovskite (Fig. 9b). This perovskite structure provides similar Area Specific Resistance as determined in literature [40].

4. Electrical and electrochemical characterizations

4.1. Electrical analyses (four points probe measurements)

In order to determine the characteristics of the well crystallized films with metallic ratio of 2, coatings deposited on alumina pellets are analyzed by four points probe measurements under oxygen gas from 293 to 1273 K at each 25 K after 20 min stabilization at each temperature. The total conductivity of the samples is calculated by equation (1).

$$\sigma = \frac{1}{\rho} = \frac{1}{4.532 * t * \frac{R_2}{R_1}} \tag{1}$$

where R1 is the electrical resistance measured at room temperature with the Jandel normed device (Ω), R2 is the electrical resistance
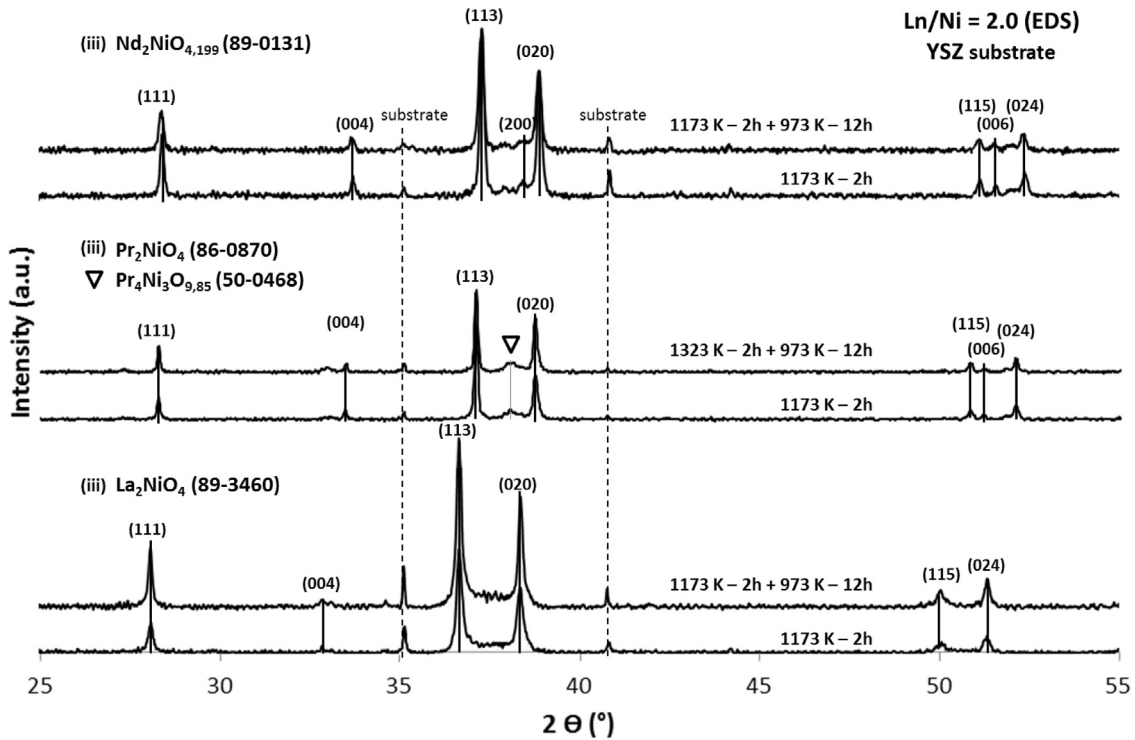
Fig. 9. XRD measurements of Ln$_2$NiO$_4$ coatings after crystallization process and after 12 h annealing process at 973 K. Ln La (a), Nd (b), Pr (c).

measured during temperature test (Ω), t represents the thickness of the coating (cm). The correction factor (4.532) depends on alumina substrate surface and the coating thickness.

The sample conductivity is plotted for the different rare earth and compared with literature data in Fig. 10. The conductivity of these samples increases with temperature and tends to be stabilized over 773 K for lanthanum and neodymium nickelate coatings, while it slightly increases for praseodymium nickelate. However, a conductivity drop happens on bulk materials (Fig. 10) contrary to thin films where conductivity continues to increase. This decrease is justified by the oxygen loss in the structure of bulk materials

[38,41,42]. Fig. 10 highlights that the electrical conductivity of the films (30−60 S cm) is in the same order of magnitude but much lower than that of bulk materials in SOFC application domain. This might be due to different microstructures, composition and/or impurities. Indeed, the results found in different studies are different even if coatings are made by the same deposition technique as shown in Fig. 10. Moreover, in literature, an Nd deficient nickelate coating provides better characteristics than a stoichiometric one [15].

The results of our study confirm the hierarchy established in literature, where the praseodymium nickelate material is the best conductor, followed by the lanthanum nickelate sample and finally by the neodymium nickelate compound [41,42]. Indeed, the conductivity of the praseodymium based deposit is similar to the lanthanum based one for the IT SOFCs' working temperature. Furthermore, Fig. 10 also shows that the conductivity of the praseodymium nickelate is higher than the neodymium and lanthanum nickelate when the temperature is lower than the operating temperature of IT SOFC. Nd$_2$NiO$_4$ material exhibits the lowest conductivity for each temperature. Electrical tests were also repeated for several cycles during the heating and the cooling stages. All the tests show the same electrical behavior with quite the same electrical conductivity values.

4.2. Electrochemical analyses (electrochemical impedance spectroscopy)

In order to determine the electrochemical performances of the well crystallized films, coatings deposited on both sides of YSZ pellet: named LN, NN, PN with Ln La, Nd and Pr respectively. Ln$_2$NiO$_4$/YSZ/Ln$_2$NiO$_4$ are analyzed by Electrochemical Impedance Spectroscopy (EIS) under air flow (60 sccm) from 873 to 1123 K at each 25 K. These tests are performed from 10 MHz to 1 Hz with 11 points per decade, and an amplitude of 0.1 V. The impedance of a

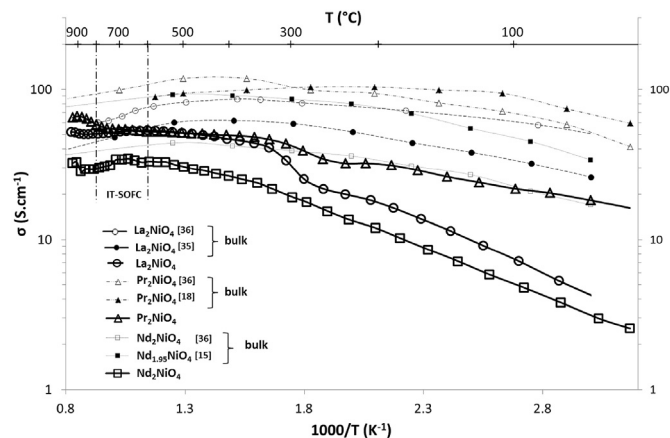**Fig. 10.** Conductivity of Ln$_2$NiO$_4$ coatings deposited on alumina substrate and previously annealed at 1173 K and 1323 K during 2 h for La$_2$NiO$_4$ and Nd$_2$NiO$_4$, Pr$_2$NiO$_4$ respectively. Measurements are performed from 293 to 1273 K with temperature steps and stabilization times of about 25 K and 20 min respectively. Ln La ($\bigcirc$), Nd ($\square$), Pr ($\blacktriangle$).

circuit presents real (Z′) and imaginary (Z″) parts as shown in (2).

$$Z(\omega) \quad Re(Z) + jIm(Z) \quad Z' + jZ'' \tag{2}$$

Impedance is usually represented in complex plan of Nyquist from equation (3).

$$Z' \quad f\left(Z''\right) \tag{3}$$

Fig. 11 represents Nyquist plots of the half cells at 973 K in order to compare the cathode behavior at IT SOFC working temperatures. Resistance is extracted from the Z axis values. It highlights huge differences between the samples in terms of resistance. It follows the same tendency as determined after electrical characterization. Indeed, the PN coating exhibits the lower resistance, followed by LN and finally NN. This hierarchy is also confirmed by literature. Nevertheless, resistances of LN and NN samples are extremely high compared to literature ones and to the PN sample. The most important difference is provided by the morphologies. Indeed, the Pr_2NiO_4 coating is porous contrary to the others as described in Fig. 8. Obtained resistances of NN and LN coatings are in the same order of magnitude than a dense LSCF coating analyzed by B. A. Boukamp et al. [43], in spite of better surface exchange and oxygen diffusion coefficients as shown in Table 1 [43].

These diagrams are fitted using Z View software. Modeled data are represented by lines in the figures while experimental mea surements are represented by points. Three contributions charac teristic of different response appearing are identified in high, medium and low frequency ranges. The resistance at high fre quencies (R_s), generally depending on the electrolyte resistance, remains the same for both samples because only the cathode layer changes. The characteristics attributed to medium or low fre quencies underline the different electrochemical response occur rence on these samples. In order to facilitate the comparisons, the resistance corresponding to high frequency signal, representing the YSZ pellet's contribution, is subtracted. Each contribution can be modeled by a sum of elementary circuits (resistance, capacitance, and inductance). Constant Phase Element function (CPE) can be used to be closer to experimental values. This function can act as a resistance, capacitance or inductance and is more and more used with electrochemical response. Resistance and associated capaci tance values were extracted from these fits. For each samples, the cathode behavior can be modeled by a sum of two R and CPE elementary circuits associated in parallel (R//CPE) and represented by a half circle in Nyquist diagrams. Two secondary circuits R//CPE express the complete behavior of the cathode layer as shown in Fig. 11 a.
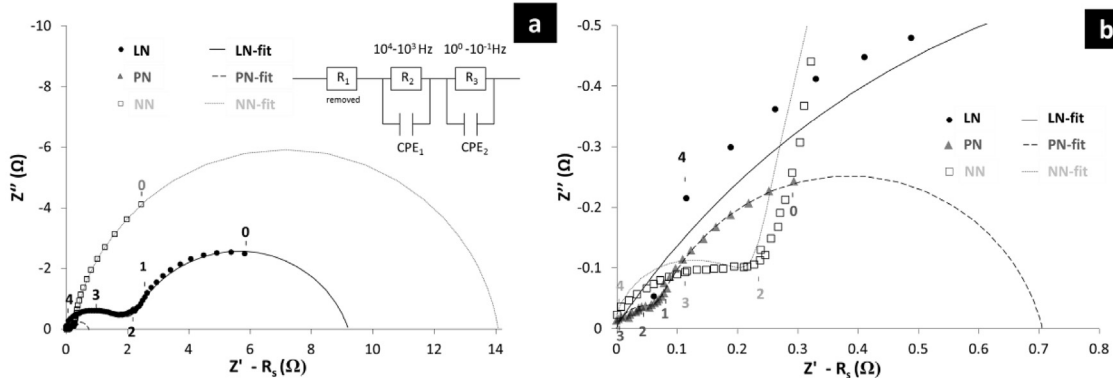
The sum of resistances allows to calculate the polarization resistance (R_p) of the cell by using equation (4) while capacities permit to identify the electrochemical response.

$$R_p \quad \left(\frac{(R_1 + R_2)*S}{2}\right) \tag{4}$$

Fig. 12 presents the polarization resistance determined from the EIS measurements from 873 to 1123 K for each sample compared to recent literature data results of Ln_2NiO_4 with YSZ electrolyte. The hierarchy determined from 973 K is similar for each temperature. The polarization resistance decreases with increasing the temper ature for PN and LN materials, while it is constant for NN material. If we compare the polarization resistance with the literature data [16,20], the LN and NN coatings present a higher value than bulk materials whereas that the PN coating is in the same order of magnitude than literature one with YSZ electrolyte. Nevertheless, resistances remain higher. The optimization of this layer could provide very interesting results. From the Arrhenius equation (5), it is possible to calculate the activation energy (E_a) of the electro chemical phenomenon by using the slope of the curve ln R f (1000/T).

$$k \quad Ae^{\frac{E_a}{RT}} \tag{5}$$

where Ea is the activation energie, R is a universal gas constant, and T is the absolute temperature.
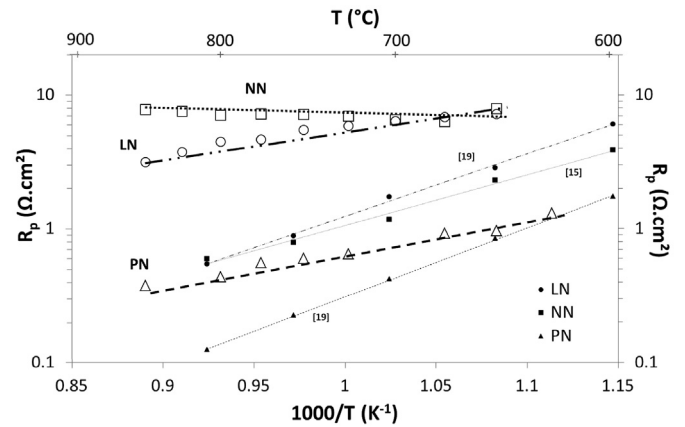
Fig. 12. Arrhenius curves of polarization resistance for the different samples from 923 K to 1123 K. LN ($\bigcirc$), NN ($\square$), PN ($\blacktriangle$).

Fig. 11. Nyquist plots of LN, NN and PN symmetrical cells deposited on YSZ at 973 K. Serial resistance is subtracted from the total resistance. Models are represented by lines. Experimental results are represented by points. Symbols represent the different samples. LN ($\bigcirc$), NN ($\square$), PN ($\blacktriangle$). Whole range of frequencies (a). Medium frequencies (b).

Table 4
Activation Energy of Ln$_2$NiO$_4$ samples.

sample	Ea calculated from Rp (eV)	Ea calculated forMF (eV)	Ea calculated for LF (eV)
LN	0.4	0.5	0.2
PN	0.6	0.8	−0.4
LN [20]	1.0		
PN [20]	1.09		
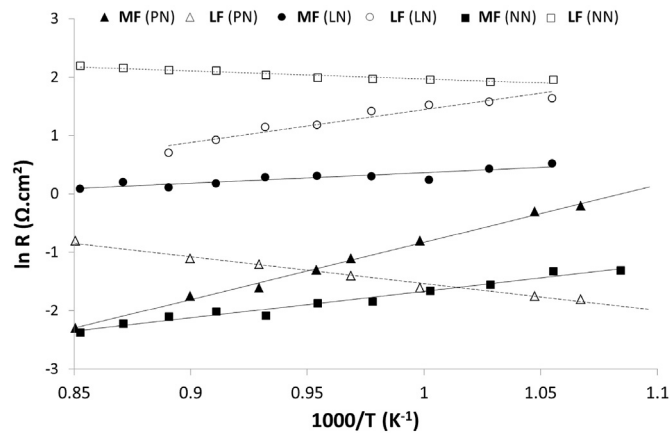
Fig. 13. Arrhenius curves of the two different resistances from 923 K to 1123 K. LN (○), NN (□), PN (▲).

Calculated activation energies are presented in Table 4. These activation energies are very low compared to literature, even with other electrolytes. Fig. 13 presents the Arrhenius plot of the different electrochemical response happening at medium fre quency range (named MF) and at low frequency range (named LF). Contrary to the LN coating where resistance decreases with tem perature for MF and LF response, the resistance of LF phenomenon increases. As a matter of fact, the activation energy is lower than it should be for the PN coating. No microstructural or structural changes have been identified after tests. The problem comes from the phenomenon appearing at low frequency. As expected after watching the polarization resistance values, the slope of the low frequency phenomenon is negative.

Using the Schouler method [44], resistance and CPE are each assigned to the resistance and capacitance that can be correlated to a specific electrochemical process. Based on the fitted data, the equivalent capacitance (Ceq) and the frequency relaxation of each contribution were calculated using equation (6).

$$C_{eq} \quad Re^{\frac{1-n}{n}}*CPE^{\frac{1}{n}} \qquad (6)$$

with R: electrical resistance, n: decentering parameter of the Constant Phase Element function, C: capacitance of the phenomenon.

According to the relaxation frequency and the equivalent capacitance values, two domains can be distinguished, at middle frequency (MF) and low frequency (LF), each representing a given electrochemical phenomenon. According to literature on cathode half cells with YSZ and GDC electrolytes, the low frequency range (LF) is characterized by high capacitance values, $C_{eq} \approx 1-10\,F\,cm^{-2}$. It was identified as the gaseous diffusion through the electrode [19,45]. The capacitance of the medium frequency contribution (MF) it was found to be larger, $C_{eq} \approx 10^{-3}\,10^{-1}\,F\,cm^{-2}$. The source of this contribution is more complicated to be identified., It has been assigned to be due to the Oxygen Reduction Reaction (ORR) occurring at the electrode/gas interface in literature [20,43] or ionic

transfers at the electrode/electrolyte interface [5]. The medium frequency phenomenon occurs at 1 kHz for LN and NN layers while it happens at 100 Hz for PN sample. The low frequency phenome non appears at 1 Hz for each coating. In literature, the behavior of LN, PN and NN coatings are generally fitted by two contributions at 100 Hz and 1 Hz respectively [12,18,19,46].

Fig. 14 presents the equivalent capacitances (C$_{eq}$) calculated from the EIS measurements, from 873 to 1173 K. The fact that these values are independent of temperature (less than two decade dif ferences in the whole range of temperature) means that it proceeds from different electrochemical contributions. These capacitances are close to literature and indicate similar response. The low frequency phenomenon indicates the same capacitances with temperature, showing similar gaseous diffusion inside the struc ture in spite of the more porous microstructure of the Pr$_2$NiO$_4$ coating. Nevertheless, as shown in Fig. 13, these similar capaci tances involve different resistances. For each material, this phe nomenon, related to electrode reaction is the limiting factor. The Medium frequency phenomenon depends on the material with values range from 10^{-3} to $10^{-5}\,F\,cm^{-2}$ but seems to be due to electrochemical processes at the electrode/electrolyte interface.

5. Conclusion

Ln$_2$NiO$_4$ coatings (Ln   La, Nd, Pr) were deposited by magnetron sputtering on different substrates by co sputtering of Ln and Ni metallic targets in presence of reactive argon oxygen gas mixtures. Using a closed loop control system, allows to obtain optimal deposition rates under chosen operational conditions. The depo sition of convenient composition coatings was performed after two steps allowing the determination of the optimal regulation point of the PEM system and the convenient intensity applied on Ni target. The optimal conditions were achieved with 70, 80 and 50% setpoint for the deposition of a transparent Ln O coating while an intensity
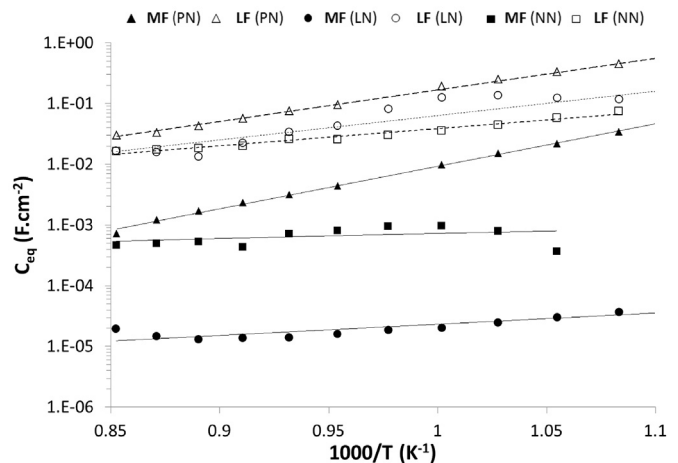
Fig. 14. Arrhenius curves of the equivalent capacities calculated from the fitting values of the Nyquist curves from 923 K to 1123 K. LN (○), NN (□), PN (▲).

of 0.57, 0.51 and 0.50 A for La, Pr and Nd targets respectively. As deposited coatings with Ln/Ni ratios of about 2 are amorphous and crystallize under a tetragonal Ln_2NiO_4 phase after an appro priate annealing treatment. A treatment under air at 1173 K for 2h is optimal for the crystallization of La Ni O and Nd Ni O coatings while the Pr_2NiO_4 phase is majoritarian at 1323 K. These different annealing treatments involve dense La_2NiO_4 and Nd_2NiO_4 coatings and nano porous Pr_2NiO_4 deposit. All of these structures are stable during 12 h at 973 K under air condition, underlining the efficiency of the crystallization step. The electrical analyses of these films deposited on alumina substrates reveal the similar behavior of the La_2NiO_4 and Pr_2NiO_4 materials in spite of different morphologies. These values (50−60 S cm in the temperature range for interme diate temperature solid oxide fuel cells) are in the same order of magnitude but lower than the most recent results obtained with these materials. The Nd_2NiO_4 material exhibits lower performances (30 S cm) as demonstrated in literature. The analysis of its elec trochemical behavior shows similar electrochemical processes with different resistances. The stability of these layers during working conditions have to be improved because some annoying increase of resistance happens on the different samples. This electrode reac tion located phenomenon should be due to Ln_2O_3 insulating pha ses, reducing the performance of these layers and lowering the calculated activation energies. The high density of the LN and NN samples implies high polarization resistances. The electrochemical response happening through the electrode were identified as the limiting factor of these cells. Contrary to the other samples, the PN material achieves similar values as literature ones and proves that the morphology of this coating facilitates the oxygen and electrons diffusion. These results are very promising for the deployment of an effective cathode material. Nevertheless, the too high crystalliza tion temperature may cause problems for its use with metal supported IT SOFCs. This study proves that the magnetron sput tering technique is efficient to deposit nanostructured MIEC cath ode materials. Nevertheless, further studies have to be done to improve the microstructure and lower the resistances.

Acknowledgements

References

[1] F. Tietz, V.A.C. Haanappel, A. Mai, J. Mertens, D. Stover, Performance of LSCF cathodes in cell tests, J. Power Sources 156 (2006) 20 22.

[2] J. Pena-Martinez, D. Marrero-Lopez, D. Pérez-Coll, J.C. Ruiz-Morales, P. Nunez, Performance of XSCoF (X Ba, La and Sm) and LSCrX'(X′ Mn, Fe and Al) perovskite-structure materials on LSGM electrolyte for IT-SOFC, Electro-chemica Acta 52 (2007) 2950 2958.

[3] K.K. Hansen, K. Vels Hansen, A-site deficient $(La_{0.6}Sr_{0.4})_{1-s}Fe_{0.8}Co_{0.2}O_{3-\delta}$ pe-rovskites as SOFC cathodes, Solid State Ionics 178 (2007) 1379 1384.

[4] J.-C. Chang, M.-C. Lee, R.-J. Yang, Y.-C. Chang, T.-N. Lin, C.-H. Wang, W.-X. Kao, L.-S. Lee, Fabrication and characterization of SDC-SSC composite cathode for anode supported solid oxide fuel cell, J. Power Sources 196 (2011) 3129 3133.

[5] J. Dailly, S. Fourcade, A. Largeteau, F. Mauvy, J.C. Grenier, M. Marrony, Perovskite and A_2MO_4-type oxides as new cathode materials for protonic solid oxide fuel cells, Electrochim. Acta 55 (2010) 5847 5853.

[6] R. Sayers, R.A. De Souza, J.A. Kilner, S.J. Skinner, Low temperature diffusion and oxygen stoichiometry in lanthanum nickelate, Solid State Ionics 181 (2010) 386 391.

[7] H. Zhao, F. Mauvy, C. Lalanne, J.-M. Bassat, S. Fourcade, J.-C. Grenier, New cathode materials for ITSOFC: phase stability, oxygen exchange and cathode properties of $La_{2-x}NiO_{4+\delta}$, Solid State Ionics 179 (2008) 2000 2005.

[8] B.C.H. Steele, K.M. Hori, S. Uchino, Kinetic parameters influencing the per-formance of IT-SOFC composite electrodes, Solid State Ionics 135 (2000) 445 450.

[9] J. Wu, X. Liu, Recent development of SOFC metallic interconnect, J. Material Sci. Technol. 26 (4) (2010) 293 305.

[10] R.J. Woolley, S.J. Skinner, Novel $La_2NiO_{4+\delta}$ and $La_4Ni_3O_{10-\delta}$ composites for

[11] R. Sayers, M. Rieu, P. Lenormand, F. Ansart, J.A. Kilner, S.J. Skinner, Develop-ment of lanthanum nickelate as a cathode for use in intermediate tempera-ture solid oxide fuel cells, Solid State Ionics 192 (2011) 531 534.

[12] F. Mauvy, J.-M. Bassat, E. Boehm, J.-P. Manaud, P. Dordor, J.-C. Grenier, Oxygen electrode reaction on $Nd_2NiO_{4+\delta}$ cathode materials: impedance spectroscopy study, Solid State Ionics 158 (2003) 17 28.

[13] D. Mesguich, J.-M. Bassat, C. Aymonier, A. Brüll, L. Dessemond, E. Djurado, Influence of crystallinity and particle size on the electrochemical properties of spray pyrolyzed $Nd_2NiO_{4+\delta}$ powders, Electrochim. Acta 87 (2013) 330 335.

[14] F. Chauveau, J. Mougin, J.-M. Bassat, F. Mauvy, J.C. Grenier, A new anode material for solid oxide electrolyser: the neodymium nickelate $Nd_2NiO_{4+\delta}$, J. Power Sources 195 (2010) 744 749.

[15] C. Lalanne, G. Prosperi, J.-M. Bassat, F. Mauvy, S. Fourcade, P. Stevens, M. Zahid, S. Diethelm, J. Van herle, J.-C. Grenier, Neodymium-deficient nickelate oxide $Nd_{1.95}NiO_{4+\delta}$ as cathode material for anode-supported intermediate temper-ature solid oxide fuel cells, J. Power Sources 185 (2008) 1218 1224.

[16] X.-D. Zhou, J.W. Templeton, Z. Nie, H. Chen, J.W. Stevenson, L.R. Pederson, Electrochemical performance and stability of the cathode for solid oxide fuel cells: V. high performance and stable Pr_2NiO_4 as the cathode for solid oxide fuel cells, Electrochim. Acta 71 (2012) 44 49.

[17] V. Vashook, E. Girdauskaite, J. Zosel, T.-L. Wen, H. Ullmann, U. Guth, Oxygen non-stoichiometry and electrical conductivity of $Pr_{2-x}Sr_xNiO_{4\pm\delta}$ with x 0 0.5, Solid State Ionics 177 (2006) 1163 1171.

[18] C. Ferchaud, J.C. Grenier, Y. Zhang-Steenwinkel, M.M.A. van Tuel, F.P.F. van Berkel, J.M. Bassat, High performance praseodymium nickelate oxide cathode for low temperature solid oxide fuel cell, J. Power Sources 196 (2011) 1872 1879.

[19] B. Philippeau, F. Mauvy, C. Matazaud, S. Fourcade, J.-C. Grenier, Comparative study of electrochemical properties of mixed conducting $Ln_2NiO_{4+\delta}$ (Ln La, Pr and Nd) and $La_{0.6}Sr_{0.4}Fe_{0.8}Co_{0.2}O_3$, Solid State Ionics 249 250 (2013) 17 25.

[20] I. Garbayo, V. Esposito, S. Sanna, A. Morata, D. Pla, L. Fonseca, N. Sabaté, A. Taracon, Porous $La_{0.6}Sr_{0.4}CoO_{3-\delta}$ thin film cathodes for large area micro solid oxide fuel cell power generators, J. Power Sources 248 (2014) 1042 1049.

[21] H.-S. Noh, K.J. Yoon, B.-K. Kim, H.-J. Je, H.-W. Lee, J.-H. Lee, J.-W. Son, The potential and challenges of thin-film electrolyte and nanostructured electrode for yttria-stabilized zirconia-base anode-supported solid oxide fuel cells, J. Power Sources 247 (2014) 105 111.

[22] T. Mukai, S. Tsukui, K. Yoshida, M. Adachi, K. Goretta, Influence of thin films structure of $Gd_{0.5}Sr_{0.5}CoO_3$ cathode on impedance spectroscopy, Electro-chem.Soc. Trans. 57 (2013) 1885 1897.

[23] K. Zhao, Y.-P. Wang, M. Chen, Q. Xu, B.-H. Kim, D.-P. Huang, Electrochemical evaluation of $La_2NiO_{4+\delta}$ as a cathode material for intermediate temperature solid oxide fuel cells, Int. J. Hydrogen Energy 39 (2014) 7120 7130.

[24] J. Fondard, P. Bertrand, A. Billard, S. Fourcade, P. Batocchi, F. Mauvy, G. Bertrand, P. Briois, Manufacturing and testing of a metal supported Ni-YSZ/YSZ/La2NiO4 IT-SOFC synthesized by physical surface deposition processes, Solid State Ionics 310 (2017) 10 23.

[25] P. Briois, A. Billard, A comparison of electrical properties of sputter-deposited electrolyte coatings dedicated to intermediate temperature solid oxide fuel cells, Surf. Coating. Technol. 201 (2006) 1328 1334.

[26] A.L. Shaula, J.C. Oliveira, V.A. Kolotygin, C. Louro, V.V. Kharton, A. Cavaleiro, Protective YSZ-based thin films deposited by RF magnetron sputtering, Vac-uum 83 (2009) 1266 1269.

[27] A. Nagata, H. Okayma, Characterization of solid oxide fuel cell device having a three-layer film structure grown by RF magnetron sputtering, Vacuum 66 (2002) 523 529.

[28] N. Jordan, W. Assenmacher, S. Uhlenbruck, V.A.C. Haanappel, H.P. Buchkremer, D. Stover, W. Mader, $Ce_{0.8}Gd_{0.2}O_{2-\delta}$ protecting layers manufactured by physical vapor deposition for IT-SOFC, Solid State Ionics 179 (2008) 919 923.

[29] A.A. Solovyev, N.S. Sochugov, S.V. Rabotkin, A.V. Shipoliva, I.V. Ionov, A.N. Kovalchuk, A.O. Borduleva, Application of PVD methods to solid oxide fuel cells, Appl. Surf. Sci. 310 (2014) 272 277.

[30] L.R. Pederson, P. Singh, X.-D. Zhou, Application of Vacuum Deposition Methods to Solid Oxide Fuel Cells, vol 80, 2006, pp. 1066 1083.

[31] P. Briois, F. Perry, A. Billard, Structural and electrical characterisation of lanthanum nickelate reactively sputter-deposited thin films, Thin Solid Films 516 (2008) 3282 3286.

[32] J. Fondard, A. Billard, G. Bertrand, P. Briois, Synthesis and characterization of $La_2NiO_{4+\delta}$ coatings deposited by reactive magnetron sputtering using plasma emission monitoring, Solid State Ionics 265 (2014) 73 79.

[33] J. Fondard, A. Billard, G. Bertrand, S. Fourcade, P. Batocchi, F. Mauvy, P. Briois, Effect of total pressure on La_2NiO_4 coatings deposited by reactive magnetron sputtering using plasma emission monitoring, Surf. Coating. Technol. 295 (2016) 29 36.

[34] A. Billard, C. Frantz, Attempted modelling of thickness and chemical hetero-geneity in coatings prepared by d.c. reactive magnetron sputtering, Surf. Coating. Technol. 59 (1993) 41 47.

[35] S. Schiller, G. Beister, W. Sieber, Reactive high rate D.C. sputtering: deposition rate, stoichiometry and features of TiO_x and TiN_x films with respect to the target mode, Thin Solid Films 111 (1984) 259 268.

[36] F. Perry, A. Billard, C. Frantz, An optical emission spectroscopy study of a reactive magnetron sputtering Ar-O_2 discharge modulated at low frequency,

solid oxide fuel cell cathodes, J. Power Sources 243 (2013) 790 795.

Surf. Coating. Technol. 94 95 (1997) 681 685.

[37] P.-L. Coddet, M.C. Pera, A. Billard, Reactive co-sputter deposition of YSZ coatings using plasma emission monitoring, Surf. Coating. Technol. 205 (2011) 3987 3991.

[38] A.V. Kovalevsky, V.V. Kharton, A.A. Yaremchenko, Y.V. Pivak, E.N. Naumovitch, J.R. Frade, Stability and oxygen transport properties of $Pr_2NiO_{4+\delta}$ ceramics, J. Eur. Ceram. Soc. 27 (2007) 4269 4272.

[39] P. Odier, C. Allançon, J.M. Bassat, Oxygen exchange in $Pr_2NiO_{4+\delta}$ at high temperature and direct formation of $Pr_4Ni_3O_{10\ x}$, J. Solid State Chem. 153 (2000) 381 385.

[40] G. Amow, I.J. Davidson, S.J. Skinner, A comparative study of the Ruddlesden-Popper series, $La_{n+1}Ni_nO_{3n+1}$ (n 1, 2 and 3), for solid-oxide fuel-cell cathode applications, Solid State Ionics 177 (2006) 1205 1210.

[41] E. Boehm, J.-M. Bassat, P. Dordor, F. Mauvy, J.-C. Grenier, Ph Stevens, Oxygen diffusion and transport properties in non-stoichiometric $Ln_{2\ x}NiO_{4+\delta}$ oxides,

Solid State Ionics 176 (2005) 2717 2725.

[42] V.V. Kharton, E.V. Tsipis, E.N. Naumovich, A. Thursfield, M.V. Patrakee, V.A. Kolotygin, J.C. Waerenborgh, I.S. Metcalfe, Mixed conductivity, oxygen permeability and redox behavior of K_2NiF_4-type $La_2Ni_{0.9}Fe_{0.1}O_{4+\delta}$, J. Solid State Chem. 181 (2008) 1425 1433.

[43] B.A. Boukamp, N. Hildebrand, P. Nammensma, D.H.A. Blank, The impedance of thin dense oxide cathodes, Solid State Ionics 192 (2011) 404 408.

[44] E.J.L. Schouler, M. Kleitz, Electrocatalysis and inductive effects at the gas Pt/Stabilized Zirconia interface, J. Electrochem. Soc. 134 (1987) 1045 1050.

[45] L. Mogni, N. Grunbaum, F. Prado, A. Caneiro, Oxygen reduction reaction on Ruddlesden-Popper phases studied by impedance spectroscopy, J. Electrochem. Soc. 158 (2011) B202 B207.

[46] M.J. Escudero, A. Aguadero, J.A. Alonso, L. Daza, A kinetic study of oxygen reduction reaction on La_2NiO_4 cathodes by means of impedance spectroscopy, J. Electroanal. Chem. 611 (2007) 107 116.